MULTI-FIELD GALERKIN LEAST-SQUARES APPROXIMATIONS FOR SMD FLUID FLOWS AROUND A CYLINDER KEPT BETWEEN PARALLEL PLATES

Daniel Dall'Onder dos Santos, dallonder@mecanica.ufrgs.br
Sérgio Frey, frey@mecanica.ufrgs.br
Laboratory of Computational and Applied Fluid Mechanics (LAMAC), Mechanical Engineering Department, Federal University of Rio Grande do Sul

Flávia Zinani, fsfzinan@ucs.br
Mechanical Engineering Department, University of Caxias do Sul

Maria Laura Martins-Costa, laura@mec.uff.br
Laboratory of Theoretical and Applied Mechanics (LMTA), Mechanical Engineering Department – PGMEC, Universidade Federal Fluminense

Abstract. *This article presents a Galerkin Least-Squares (GLS) finite element multifield formulation – considering three primal variables: extra-stress, velocity and pressure – for modeling viscoplastic fluids flowing around a cylinder confined between parallel plates. The recently proposed viscoplastic constitutive equation – henceforth simply called SMD model – is assumed, predicting shear-thinning and yield stress fluid behavior. The mechanical model is approximated by the GLS method, which circumvents the need to satisfy the compatibility condition known as Babuška-Brezzi condition and also the compatibility condition between extra-stress and velocity subspaces, which arises for multi-field formulations. Some bi-dimensional numerical results, assuming inertialess fluid flows, have been obtained for velocity, pressure and extra-stress fields with the studied geometry, in which the dimensionless viscoplastic number of the SMD model, namely the jump number J, as ranged from 1 to 1000 and the power-law exponent from 0.5 to 1.5. As it was verified by computational tests, the unyielded regions of the material decreases with the increase of the jump number, the pressure drop on the plate increases with the increasing of the power-law coefficient and the axial velocity profiles become flatter as the coefficient n decreases.*

Keywords: *Non-Newtonian fluids; Viscoplastic fluid flows; SMD model; Multi-field formulation; Galerkin least-squares method*

1. INTRODUCTION

Viscoplastic fluid behavior is exhibited by several materials including drilling muds and heavy oils in the petroleum industry, mayonnaise, creams and many dairy products in the food and cosmetics industries, clay, and concentrated suspensions, and so on. Many models have been proposed along the past years to approximate the yield-stress behavior, like Bingham, Casson and Herschel-Bulkley models. Analytical solutions were provided for these models in simple shear flows. Souza Mendes and Dutra, based on recent rheological measurements of the behavior of viscoplastic fluids subjected to very low shear stresses, introduced a model in 2004 – from now on denoted as SMD (Souza Mendes and Dutra, 2004) – which aims to represent the behavior of viscoplastic real liquids more realistically. This model regularizes the shear stress field by employing rheological parameters only.

The main purpose of this paper is to study viscoplastic fluid flows using a multi-field Galerkin least-squares (GLS) finite element formulation which takes into account velocity, pressure and extra-stress fields as primal variables. The classical Galerkin method does not guarantee stable approximations, may generate solutions without physical meaning and numerical pathologies for mixed incompressible fluid flows, such as the locking of the velocity field and spurious oscillations on the pressure field. The inherent difficulties associated to the Galerkin method are due to the compatibility of velocity and pressure finite element subspaces, e. g., the need to satisfy the Babuška-Brezzi condition involving these subspaces, a condition which was established by Babuška and Brezzi in the early 70's – see, for details, Babuška (1973) and Brezzi (1974). According to these works, the velocity and pressure subspaces may not be spanned by any arbitrary combination of finite element interpolations and, in the case of multi-field formulations, another compatibility condition must be imposed on the choice of the stress and velocity subspaces. Besides, if the inertia effects are taken into account, the classical Galerkin method fails to capture stably high advective flows due to the unsymmetrical nature of the advective terms of motion equation. This latter shortcoming is even more felt in flows of shear-thinning viscoplastic fluids, for which the apparent fluid viscosity experiments severe gradients near the geometry boundary and near the yield surface.

The alternatives to remedy Galerkin deficiencies in incompressible fluid flows may be accommodated, in a simple way, in the follow duality: either to hold the classical Galerkin formulation employing no-conforming finite elements or to change Galerkin formulation and use simple Lagragean elements. It is in that alternative in which the GLS method must be viewed, a methodology whose major features are enhancing Galerkin stability with usual combinations of finite elements – for instance, equal-order elements, a very attractive combination from the computational point-of view-without upsetting its consistency.

The dimensionless viscoplastic number of the SMD model, namely the jump number J, introduced by Souza Mendes et al., (2007) and the power-law index were ranged in order to investigate the flow dynamics of non-linear viscoplastic materials. The numerical computations, considering steady-state creeping flow, have been carried out for power-law indexes ranging from 0.5 to 1.5, the dimensionless parameter J varying from zero to 1000 and inlet dimensionless average velocity from 0.5 to 2.0. The numerical results generated by the GLS approximations were physically coherent with the flow dynamics of the problem, being in accordance with the literature.

2. MECHANICAL MODEL

The mechanical model combines the principles of mass and linear momentum balances for a steady-state flow of an incompressible fluid through an open domain $\Omega \subset \Re^{N=2,3}$ with a regular boundary *Γ*,

$$\begin{aligned} &\rho[\nabla \mathbf{u}]\mathbf{u} - \operatorname{div} \mathbf{T} = \mathbf{f} && \text{in } \Omega \\ &\operatorname{div} \mathbf{u} = 0 && \text{in } \Omega \end{aligned} \tag{1}$$

In Eq. (1) u represents the fluid velocity, r its mass density, f the body force per unit mass and the stress tensor T may be decomposed into a hydrostatic and viscous portions, T=-p**I**+$\boldsymbol{\tau}$

Constitutive equations for the stress tensor must satisfy some requirements (Astarita and Marrucci, 1974), namely the principles of determinism, local action and frame indifference, and the second law of Thermodynamics. The principles of determinism and local action are satisfied if the stress **T** is expressed as a function of the fluid velocity **u** and its gradient **L**, i. e., **T** = **H**(**u**, **L**). However, neither the vector **u** nor the tensor **L** are frame indifferent quantities. If frame indifference is also applied, it may be proved that the tensor **T** must be only dependent of the tensor **D**, the symmetrical part of tensor **L**, i. e., **T**=**G**(**D**) (see, for instance, Astarita and Marrucci, 1974).

The most general form to relate the tensor **T** to the flow kinematics is the Reiner-Prager equation (Slattery, 1999),

$$\mathbf{T} = -\phi_0 \mathbf{1} + \phi_1 \mathbf{D} + \phi_2 \mathbf{D}^2 \tag{2}$$

with the scalars $\phi_i = \phi_i(I_{\mathbf{D}}, II_{\mathbf{D}}, III_{\mathbf{D}}),\ i = 0.1,2$ being functions of the principal invariants of tensor **D**,

$$I_{\mathbf{D}} = \operatorname{tr} \mathbf{D} \ , \quad II_{\mathbf{D}} = \frac{1}{2}[I_{\mathbf{D}}^2 \text{ - } \operatorname{tr} \mathbf{D}^2] \ , \quad III_{\mathbf{D}} = \det \mathbf{D} \tag{3}$$

Assuming that **T** obeys the generalized Newtonian liquid (GNL) model (Bird *et al.*, 1987), $\mathbf{T} = -p\mathbf{1} + \boldsymbol{\tau} = -p\mathbf{1} + 2\eta(\dot{\gamma})\mathbf{D}$, where the viscosity function η is dependent of $\dot{\gamma}$, the magnitude of the rate of strain tensor **D**, $\dot{\gamma} = (2 \operatorname{tr} \mathbf{D}^2)^{1/2}$.

The SMD model proposed by Souza Mendes and Dutra (2004), adequate for describing highly pseudoplastic liquids, regularizes the shear stress field employing rheological parameters only, namely the yield stress, τ_0, the zero-shear-rate viscosity, η_0, the consistency index, *K*, and the power-law index, *n*. It predicts the following expressions for shear stress and viscosity function:

$$\begin{aligned} &\tau = (\tau_0 + K(\dot{\gamma})^n)(1 - \exp(-\eta_0 \dot{\gamma}/\tau_0)) \\ &\eta(\dot{\gamma}) = (\tau_0/\dot{\gamma} + K(\dot{\gamma})^{(n-1)})(1 - \exp(-\eta_0 \dot{\gamma}/\tau_0)) \end{aligned} \tag{4}$$

Next, in Souza Mendes *et al.* (2007), the authors introduced a rheological dimensionless property for viscoplastic fluids – the so-called jump number J, which provides “a relative measure of the jump in the shear rate when the shear stress is approximately equal to the stress limit, $\tau \approx \tau_0$ ”. Mathematically, it may be defined as:

$$\mathrm{J} = \frac{\dot{\gamma}_1 - \dot{\gamma}_0}{\dot{\gamma}_0} = \frac{(\tau_0/K)^{1/n} - \tau_0/\eta_0}{\tau_0/\eta_0} = \eta_0 \left(\frac{\tau_0^{1-n}}{K} \right)^{1/n} - 1 \tag{5}$$

in which $\dot{\gamma}_0$ is the shear rate value at the beginning of the shear rate jump and $\dot{\gamma}_1$ the shear rate value for which the power-law region begins – see Fig. 1(a)-(b) for details. Still in this article, introducing the dimensionless quantities $\dot{\gamma}^*=\dot{\gamma}/\dot{\gamma}_1$ and $\tau^*=\tau/\tau_0$, the authors have obtained the following dimensionless shear stress and viscosity equations:

$$
\begin{aligned}
&\tau^*=(1-\exp[-(J+1)\dot{\gamma}^*])[1+\dot{\gamma}^{*^n}]\\
&\eta^*\equiv\frac{\tau^*}{\dot{\gamma}^*}=(1-\exp[-(J+1)\dot{\gamma}^*])[\frac{1}{\dot{\gamma}^*}+\dot{\gamma}^{*^{(n-1)}}]
\end{aligned}
\tag{6}
$$

Figure 1 shows the influence of the jump number J – defined in Eq. (5) – on the SMD flow curve (Fig.1(a)) and on the SMD viscosity function (Fig.1(b)). It may be noticed that as the the jump number grows, the SMD model mimics the classical Herschel-Bulkley (Fig.1(a)) and the low shear rate viscosity tends to infinite (Fig.1(b)) .

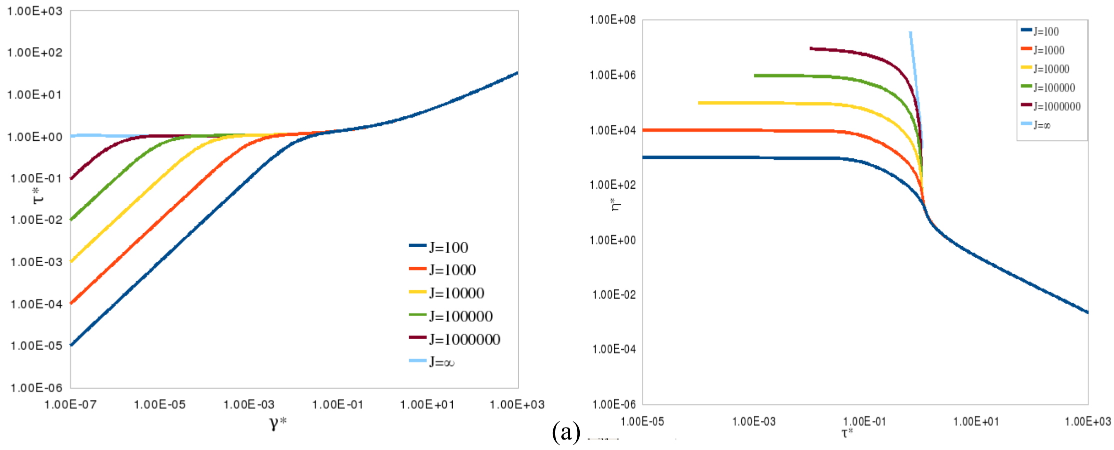

(a) (b)

Figure 1: Influence of the jump number J (a) on the SMD flow curve and (b) on the SMD viscosity function.

3. NUMERICAL APPROXIMATION

The multi-field boundary value problem, concerns the viscoplastic fluid flow defined by the triple shear stress, pressure and velocity fields and the associated system of contact and body forces – namely mass and momentum balance equations, Eq.(1) – coupled with the SMD constitutive model for viscoplasticity defined by Eq.(6) and also accounting for the boundary conditions, may be stated as:

$$
\begin{aligned}
&\rho[\nabla\mathbf{u}]\mathbf{u}-\operatorname{div}\boldsymbol{\tau}+\nabla p=\mathbf{f} && \text{in } \Omega\\
&\boldsymbol{\tau}-2\eta(\dot{\gamma})\mathbf{D}(\mathbf{u})=0 && \text{in } \Omega\\
&\operatorname{div}\mathbf{u}=0 && \text{in } \Omega\\
&\mathbf{u}=\mathbf{u}_g && \text{on } \Gamma_g\\
&[-p\mathbf{I}+\boldsymbol{\tau}]\mathbf{n}=\mathbf{t}_h && \text{on } \Gamma_h
\end{aligned}
\tag{7}
$$

where Γ_g is the portion of the boundary Γ on which Dirichlet condition is imposed and Γ_h the portion on which Neumann condition is imposed, $\mathbf{u}_g$ a prescribed velocity field, $\mathbf{t}_h$ the stress vector and $\eta(\dot{\gamma})$ is the SMD viscosity function given by Eq. (6). The remaining variables have been previously defined.

The finite element approximation is based on a usual finite element partition, employing the finite element subspaces for shear stress ($\boldsymbol{\Sigma}^h$), velocity ($\mathbf{V}^h$) and pressure (P^h) fields presented below:

$$
\begin{aligned}
&\mathbf{V}^h=\{\mathbf{v}\in H_0^1(\Omega)^N|\mathbf{v}_K\in R_k(K)^N,\ \ K\in\Omega^h\}\\
&\mathbf{V}_g^h=\{\mathbf{v}\in H^1(\Omega)^N|\mathbf{v}_K\in R_k(K)^N,\ \ K\in\Omega^h,\ \ \mathbf{v}=\mathbf{u}_g \text{ on } \Gamma_g\}\\
&P^h=\{p\in C^0(\Omega)\cap L_2^0(\Omega)|p_K\in R_l(K),\ \ K\in\Omega^h\}\\
&\boldsymbol{\Sigma}^h=\{\mathbf{S}\in\boldsymbol{\Sigma}|\mathbf{S}_K\in R_m(K)^{NxN},\ \ K\in\Omega^h\}\\
&\boldsymbol{\Sigma}=\{\mathbf{S}\in C^0(\Omega)^{NxN}\cap L_2(\Omega)^{NxN}|S_{ij}=S_{ji},\ \ i,j=1,\dots,N\}
\end{aligned}
\tag{8}
$$

where $C^0(\Omega)$ represents the space of continuous functions, $L^2(\Omega)$ the Hilbert space of square integrable functions in Ω, $H^1(\Omega)$ the Sobolev functional space of functions with square integrable value and derivatives in Ω, R_k, R_l and R_m the polynomial spaces of degree in k, l and m, respectively, in Ω^h and N represents the number of space dimensions considered in the problem.

3.1 Multi-field Galerkin least-squares formulation

Based on the finite element subspaces defined by Eq. (8), a multi-field Galerkin least-squares formulation for the system defined by Eq. (7) may be written as: *Find* $(\boldsymbol{\tau}^h, p^h, \mathbf{u}^h) \in \boldsymbol{\Sigma}^h \mathrm{x} P^h \mathrm{x} \mathbf{V}_g^h$ *such that*

$$B(\boldsymbol{\tau}^h, p^h, \mathbf{u}^h; \mathbf{S}^h, q^h, \mathbf{v}^h) = F(\mathbf{S}^h, q^h, \mathbf{v}^h) \qquad \forall (\mathbf{S}^h, q^h, \mathbf{v}^h) \in \boldsymbol{\Sigma}^h \times P^h \times \mathbf{V}_g^h \tag{9}$$

where

$$\begin{aligned} B(\boldsymbol{\tau}^h, p^h, \mathbf{u}^h; \mathbf{S}^h, q^h, \mathbf{v}^h) = & \frac{1}{2\eta(\dot{\gamma})} \int_\Omega \boldsymbol{\tau}^h \cdot \mathbf{S}^h d\Omega - \int_\Omega \mathbf{D}(\mathbf{u})^h \cdot \mathbf{S}^h d\Omega \\ & + \int_\Omega \rho([\nabla \mathbf{u}^h]\mathbf{u}^h) \cdot \mathbf{v}^h d\Omega + \int_\Omega \boldsymbol{\tau} \cdot \mathbf{D}(\mathbf{v}^h) d\Omega - \int_\Omega p \operatorname{div} \mathbf{v}^h d\Omega + \int_\Omega \operatorname{div} \mathbf{u}^h q^h d\Omega + \epsilon \int_\Omega p^h q^h d\Omega \\ & + \sum_{K \in \Omega^h} \int_{\Omega_K} (\rho[\nabla \mathbf{u}^h]\mathbf{u}^h + \nabla p^h - \operatorname{div} \boldsymbol{\tau}) . \alpha(\mathrm{Re}_K)(\rho[\nabla \mathbf{v}^h]\mathbf{u}^h + \nabla q^h - \operatorname{div} \mathbf{S}^h) d\Omega \\ & + 2\eta(\dot{\gamma})\beta \int_\Omega (\frac{1}{2\eta(\dot{\gamma})}\boldsymbol{\tau}^h - \mathbf{D}(\mathbf{u})^h).(\frac{1}{2\eta(\dot{\gamma})}\mathbf{S}^h - \mathbf{D}(\mathbf{v})^h) d\Omega + \delta \int_\Omega \operatorname{div} \mathbf{u}^h \operatorname{div} \mathbf{v}^h d\Omega \end{aligned} \tag{10}$$

and

$$\begin{aligned} F(\mathbf{S}^h, q^h, \mathbf{v}^h) = & \int_\Omega \mathbf{f} \cdot \mathbf{v}^h d\Omega + \int_{\Gamma_h} \mathbf{t}_h \cdot \mathbf{v}^h d\Gamma \\ & + \sum_{K \in \Omega^h} \int_{\Omega_K} \mathbf{f} \cdot (\alpha(\mathrm{Re}_K)(\rho[\nabla \mathbf{v}^h]\mathbf{u}^h + \nabla q^h - \operatorname{div} \mathbf{S})) d\Omega \end{aligned} \tag{11}$$

where the positive constant scalar β multiplying the least-squares of the viscoplastic model is taken as proposed in Behr *et al.*, (1993), i. e., $0<\beta<1$ and the stability parameters multiplying the least-squares of motion and continuity equation, $\alpha(\mathrm{Re}_K)$ and δ respectively, are given as in Franca and Frey (1992),

$$\begin{aligned} & \alpha(\mathrm{Re}_K) = \frac{h_K}{2|\mathbf{u}|_p} \xi(\mathrm{Re}_K) \qquad \delta = \chi |\mathbf{u}|_p h_K \xi(\mathrm{Re}_K) \quad \text{with} \quad \xi(\mathrm{Re}_K) = \begin{cases} \mathrm{Re}_K, & 0 < \mathrm{Re}_K < 1 \\ 1, & \mathrm{Re}_K > 1 \end{cases} \\ & \mathrm{Re}_K = \frac{\rho m_k |\mathbf{u}|_p h_K}{4\eta(\dot{\gamma})} \quad \text{with} \quad m_k = \min\{1/3, 2C_k\} \quad \text{and} \quad C_k \sum_{K \in \Omega^h} h_K^2 \|\operatorname{div} \mathbf{D}(\mathbf{u})^h\|_{0,K}^2 \le \|\mathbf{D}(\mathbf{u})^h\|_0^2 \quad \forall \mathbf{u}^h \in \mathbf{V}^h \end{aligned} \tag{12}$$

Remarks:

1. The multi-field GLS formulation defined by Eq. (9)-(11) is formed by the addition of the least-squares terms of the motion and continuity balance equation (Eq. (1)) and the viscoplastic model (Eq. (6)) to the classical Galerkin formulation.
2. The GLS formulation defined by Eqs.(9)-(11) is identical to a GLS formulation proposed by Behr *et al.* (1993) for context of constant viscosity fluids. Furthermore, if we drop the inertia terms, *i.e.*, Re=0, the formulation of Franca and Stenberg (1991) is recovered.

3.2. Matrix problem

Introducing the shape functions for $\boldsymbol{\tau}^h$, $\mathbf{u}^h$, p^h, $\mathbf{S}^h$, $\mathbf{v}^h$ and q^h in the GLS formulation presented in Eqs. (9)-(11), the following residual equation is obtained:

$$\mathbf{R}(\mathbf{U}) = \mathbf{0} \tag{13}$$

where $\mathbf{U}^h$ is the vector of degrees of freedom of $\boldsymbol{\tau}^h$, $\mathbf{u}^h$ and p^h given by $\mathbf{U}^h = [\boldsymbol{\tau}^h, \mathbf{u}^h, \boldsymbol{p}^h]^T$

$$\mathbf{R}(\mathbf{U})=[(1+\beta)\mathbf{E}(\eta(\dot{\gamma}))+(1-\beta)\mathbf{H}+\mathbf{E}_{\alpha}(\eta(\dot{\gamma}),\mathbf{u})]\boldsymbol{\tau}+[\mathbf{N}(\mathbf{u})+\mathbf{N}_{\alpha}(\eta(\dot{\gamma}),\mathbf{u})+\beta\mathbf{K}-(1+\beta)\mathbf{H}^{T}-\mathbf{G}^{T}+\mathbf{M}]\mathbf{u}$$
$$[\mathbf{G}+\mathbf{G}_{\alpha}(\eta(\dot{\gamma}),\mathbf{u})+\mathbf{P}]\mathbf{p}-\mathbf{F}-\mathbf{F}_{\alpha}(\eta(\dot{\gamma}),\mathbf{u}) \quad (14)$$

where [**H**] and [$\mathbf{H}^T$] are the matrices representing the coupling between $\boldsymbol{\tau}$ and **u**, [**E**] is the matrix related to the extra-stress $\boldsymbol{\tau}$ term, [**N**] is the matrix of advective terms, [**K**] is the matrix of diffusive terms, [**G**] is the matrix of pressure terms, [$\mathbf{G}^T$] the matrix of continuity equation term and [**F**] is the body forces term matrix. The matrices with subscript α – namely [$\mathbf{E}_\alpha$], [$\mathbf{N}_\alpha$], [$\mathbf{G}_\alpha$], and [$\mathbf{F}_\alpha$] are the matrices originated from the GLS terms. Also, [**M**] is the matrix of the δ term and [**P**] is the matrix of the ε term in Eq. (9)-(11).

To solve the non-linear matrix problem defined by Eq. (13)-(14) an incremental quasi-Newton method has been implemented where the Jacobian matrix was updated only at each two or three iterations (Zinani and Frey, 2008) . The algorithm requires a initial guess $\mathbf{U}_0^h$ and, at each iteration, we solve the linear system

$$\mathbf{J}(\mathbf{U}_k^h)\Delta\mathbf{U}_{k+1}^h=-\mathbf{R}(\mathbf{U}_k^h) \quad (15)$$

where $\mathbf{R}(\mathbf{U}_k^h)$ is given by Eq.(14) and the Jacobian matrix $\mathbf{J}(\mathbf{U}_k^h)$ calculated analytically,

$$\mathbf{J}(\mathbf{U}_k^h)=\frac{\partial\mathbf{R}(\mathbf{U}_k^h)}{\partial\mathbf{U}_k^h} \quad (16)$$

in order to find the incremental vector $\Delta\mathbf{U}_{k+1}^h$ and to compute

$$\mathbf{U}_{k+1}^h=\mathbf{U}_k^h+\Delta\mathbf{U}_{k+1}^h \quad (17)$$

We assume that convergence is achieved when $\left|\mathbf{R}(\mathbf{U}_k^h)\right|_\infty<\epsilon$ – in this work, we take $\epsilon=10^{-7}$.

4. NUMERICAL RESULTS

The GLS formulation presented in Eqs. (9)-(11) was used to simulate inertialess flows of SMD fluids around a cylinder kept between parallel plates. The problem statement consists of a cylinder with unitary radius inserted into parallel layers distant one unity from the cylinder surface. Since this geometry is symmetrical, only half of the computational domain was simulated, as shown in Fig. 2. Impermeability and no-slip conditions at the channel walls and at the cylinder surface; zero vertical velocity and transversal gradient of horizontal velocity at the centerline as well as an uniform horizontal velocity profile at inlet and outlet were the imposed boundary conditions. All the computations have been performed with the finite element code for fluids under development at Laboratory of Computational and Applied Fluid Mechanics (LAMAC-UFRGS).

The partitioning of the computational domain in 11,584 quadrilateral bilinear elements (Q1/Q1) has been considered generating 11,957 nodal points. At the cylinder surroundings, the mesh is more refined in order to better characterize the yielded surfaces downstream and upstream the cylinder, as depicted in Fig. (3).

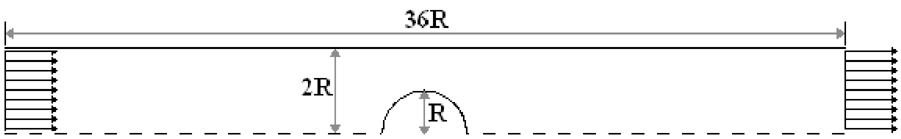

Figure 2: Problem statement: Cylinder kept between parallel plates.

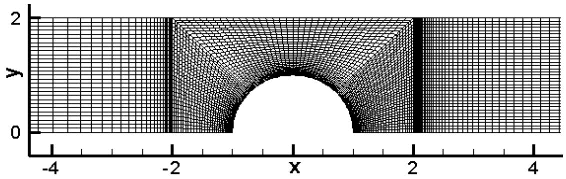

Figure 3: Employed Mesh.

The inlet dimensionless average velocity is defined as $\bar{u}_{in}^{*} = u_{in} / (\dot{\gamma}_1 2\mathrm{R})$ – with u_{in} representing the imposed inlet velocity, 2R half the channel height and $\dot{\gamma}_1$ the shear rate value at the power-law region. In all computations, it is assumed creeping flow, i. e., the Reynolds number is taken as zero. Figure 4 compares pressure elevation considering the jump number J=1000, *n*=1 and $\bar{u}_{in}^{*} = 1.0$, obtained by classical Galerkin and GLS methods, for the refined mesh presented in Fig. 3, showing spurious oscillations in the former methodology.

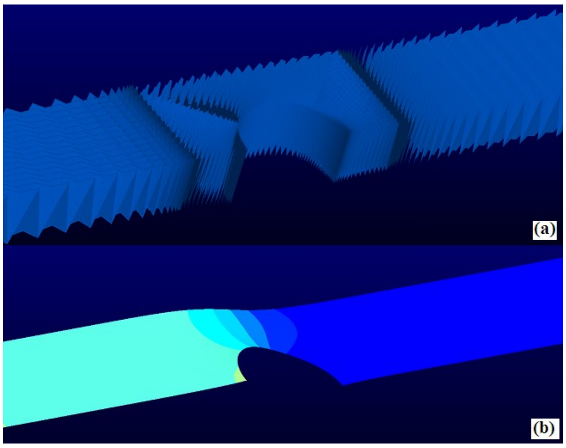

Figure 4. Pressure elevation for J=1000, $\bar{u}_{in}^{*} = 1.0$; *n*=1, and equal-order elements: (a) Galerkin; (b): GLS.

Figure 5 shows the influence of the jump number on yielded and unyielded regions, considering *n*=0.5 and $\bar{u}_{in}^{*} = 1.0$, ranging J from 0 to 100. From the figure, as the jump number increases the unyielded zones decrease; the polar caps – barely visible for J=0 and J=1 depicted in Fig. 5(a) Fig. 5(b), respectively – vanish for J greater or equal than 5 (Fig. 5(c)-Fig. 5(f)). Also, the islands (over the cylinder) decrease as J increases.

Figure 6 presents the influence of J number on τ_{12}-isobands, for *n*=0.5 and $\bar{u}_{in}^{*} = 1.0$ and varying the jump number from J=0 to J=100. As it may be viewed, the shear stress plotting is only a matter of a trivial graphical post-processing when a multi-field formulation has been employed, since τ is a primal variable for this kind of formulation.

Figure 7 shows the influence of the power-law index on the pressure elevation plots, for values of J=10 and $\bar{u}_{in}^{*} = 1$, with the power-law index *n* ranging from *n*=0.5, 1.0 and 1.5. The figure allows to conclude that as the power coefficient *n* increases, the pressure drop increases too, due to shear-thinning effects.

Finally, Fig. 8 illustrates the influence of *n* index on the horizontal and vertical velocity elevation plots, considering J=10 and $\bar{u}_{in}^{*} = 1.0$. Figures 8(a)-8(c), for horizontal velocity elevations, show that the maximum axial velocity over the cylinder increases as the *n* index grows, while Fig. 8(d)-8(f), for vertical velocity elevations, illustrate no visible influence of the *n* index on axial velocity elevations upstream and downstream the cylinder.

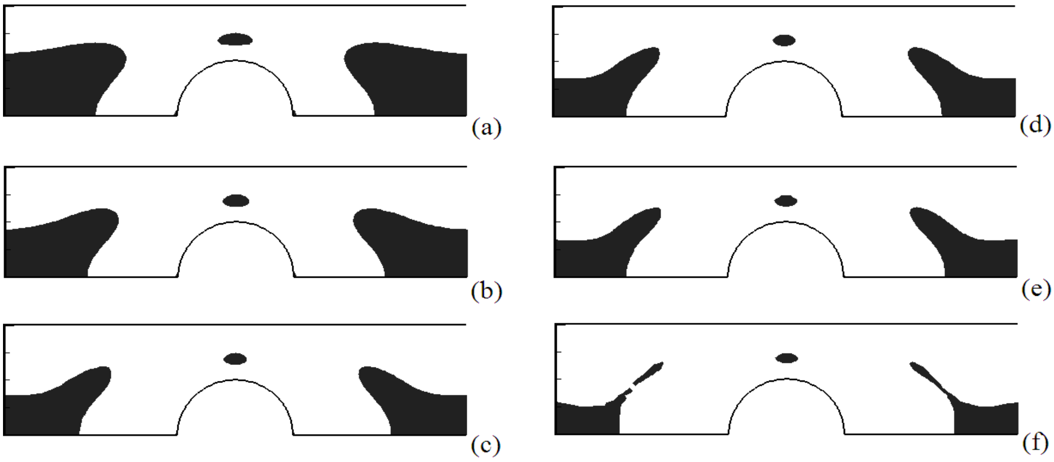

Figure 5: Yielded and unyielded zones for n=0.5 and $\bar{u}^*_{in} = 1.0$ ranging the jump number: (a) J=0; (b) J=1; (c) J=5; (d) J=7.5; (e) J=10;(f) J=100.

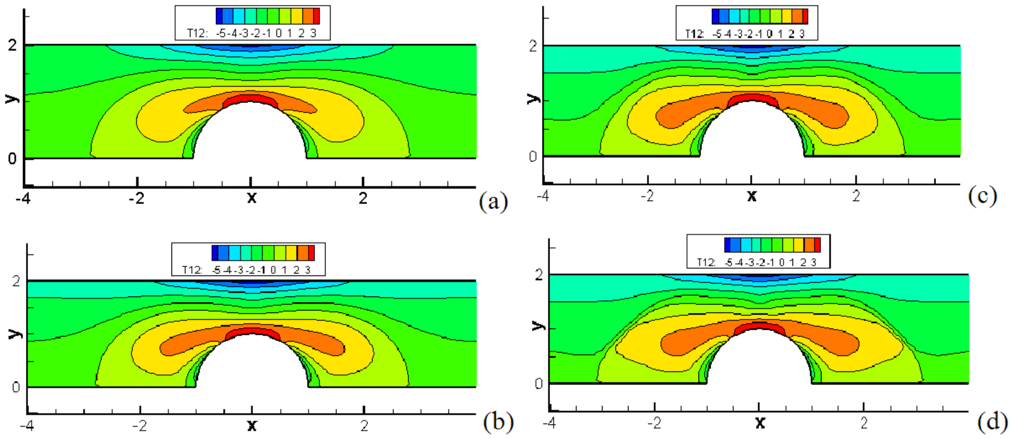

Figure 6: Influence of J number on τ_{12}-isobands considering n=0.5 and $\bar{u}^*_{in} = 1.0$: for (a) J=0; (b) J=1; (c) J=10; (d) J=100.

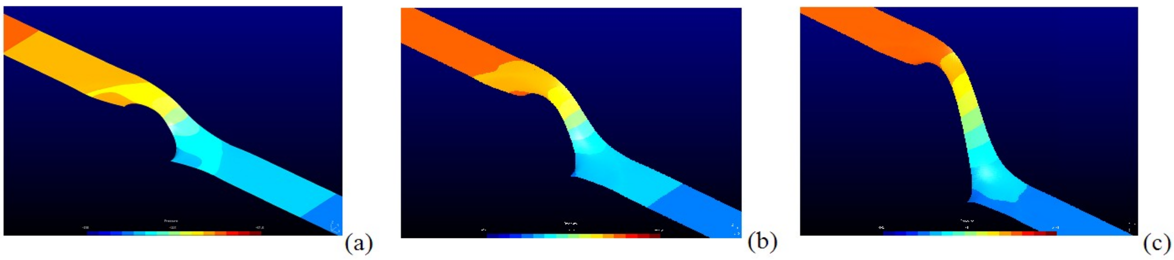

Figure 7: Influence of n index on pressure elevation, for $\bar{u}^*_{in} = 1.0$ and J=10: (a) n=0.5, (b) n=1.0 and (c) n=1.5.

5. FINAL REMARKS

This work presented a multi-field (extra-stress, velocity and pressure fields) Galerkin least-squares formulation for SMD fluids flowing around a cylinder confined between parallel plates. The GLS formulation was enough stable to approximate inelastic non-Newtonian fluid flows, characterized by shear-rate dependent viscosity and yield limit, even employing an equal-order combination of velocity and pressure subspaces. From the numerical viewpoint, the use a multi-field GLS formulation had the advantage of a simple computational implementation, being directly extended for three-dimensional situations. Due to shear-thinning and viscoplastic material behavior, the flow dynamics differs very much from the Newtonian ones. For creeping flows, unyielded zones decrease with the increasing of J number, the increase of the *n* index increases the pressure drop and the axial velocity profiles become more elongated.

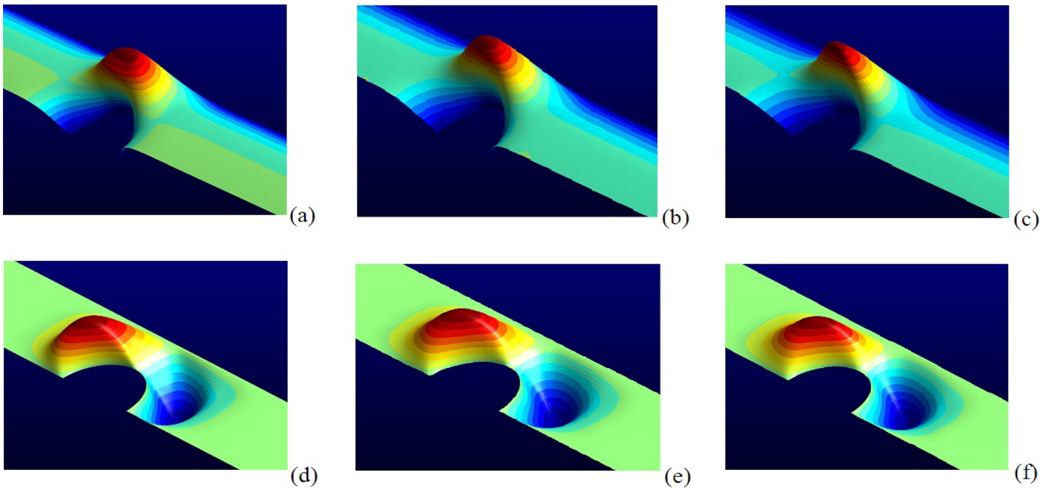

Figure 8: Influence of *n* index, for J=10 and $\bar{u}_{in}^* = 1.0$, on the horizontal – (a) *n*=0.5, (b) *n*=1.0, (c) *n*=1.5 – and vertical – (d) *n*=0.5, (e) *n*=1.0, (f) *n*=1.5 – velocity elevations.

6. ACKNOWLEDGEMENTS

The author D. Dall'Onder dos Santos thanks for its scholarship provided by FAPERGS, the authors S. Frey and M.L. Martins-Costa acknowledge CNPq for financial support and grants.

7. REFERENCES

Astarita, G., Marrucci, G., 1974. “Principles of non-Newtonian fluid mechanics”. McGraw-Hill, Great Britain.
Babuška I., 1973. “The finite element method with Lagrangean multipliers”. vol. 20, pp.179-192.
Behr, M., Franca, L.P., Tezduyar, T.E., 1993. “Stabilized finite element methods for the velocity-pressure-stress formulation of incompressible flows”, Comput. Methods Appl. Mech. Engrg., vol. 104, pp. 31-48.
Bird, R. B., Armstrong, R. C., Hassager, O., 1987. “Dynamics of Polymeric Liquids”. Vol. 1, John Wiley & Sons, U.S.A.
Brezzi F., 1974. “On the existence, uniqueness and approximation of saddle-point problems arising from Lagrange multipliers”, RAIRO Anal. Numér., vol. 8, pp. 129-151.
Franca, L.P., and Frey, S., 1992, “Stabilized finite element methods: II. The incompressible Navier-Stokes equations”, Comput. Methods Appl. Mech. Engrg., vol. 99, pp. 209-233.
Franca, L.P., Stenberg, R., 1991. “Error Analysis of Some Galerkin Least Squares Methods for the Elasticity Equations”, SIAM J. Numer. Anal., 28(6), pp. 1680-1697.
Slattery, J. C., 1999. “Advanced transport phenomena”. Cambridge University Press, U.S.A.
Souza Mendes, P.R. and Dutra, E.S.S., 2004. “Viscosity function for yield-stress liquids”, Applied Rheology, Vol. 14, pp. 296-302.
Souza Mendes, P.R., Naccache, M.F, Varges, P.R. and Marchesini, F.H., 2007. “Flow of viscoplastic liquids through axisymmetric expansions-contractions”, J. Non-Newtonian Fluid Mech., Vol. 142, pp. 207-217.
Zinani, F., Frey, S., 2008, “Galerkin Least-Squares Multi-Field Approximations for Flows of Inelastic non-Newtonian Fluids”, J. Fluids Engng. – Trans. ASME, to appear.

8. RESPONSIBILITY NOTICE

The authors are the only responsible for the printed material included in this paper.